

Phonons in nanocrystalline Ni₃Fe

H. Frase and B. Fultz

Division of Engineering and Applied Science, 138-78, California Institute of Technology, Pasadena, California 91125

J. L. Robertson

Oak Ridge National Laboratory, P.O. Box 2008, Oak Ridge, Tennessee 37831

(Received 2 September 1997)

Inelastic neutron-scattering spectra were measured to obtain the phonon density of states (DOS) of nanocrystalline fcc Ni₃Fe. The materials were prepared by mechanical alloying, and were also subjected to heat treatments to alter their crystallite sizes and internal strains. In comparison to material with large crystallites, the nanocrystalline material shows two distinct differences in its phonon DOS. The nanocrystalline DOS was more than twice as large at energies below 15 meV. This increase was approximately proportional to the density of grain boundaries in the material. Second, features in the nanocrystalline DOS are broadened substantially. This broadening did not depend in a simple way on the crystallite size of the sample, suggesting that it has a different physical origin than the enhancement in phonon DOS at energies below 15 meV. A damped harmonic oscillator model for the phonons provides a quality factor Q_u , as low as 7 for phonons in the nanocrystalline material. The difference in vibrational entropy of the bulk and nanocrystalline Ni₃Fe was small, owing to competing changes in the nanocrystalline phonon DOS at low and high energies. [S0163-1829(98)06402-9]

I. INTRODUCTION

Nanocrystalline materials, often defined as materials composed of crystallites smaller than 100 nm, have attracted much interest in the past decade. Unusual mechanical properties and soft magnetic properties have motivated numerous investigations on metallic nanocrystals.^{1,2} The synthesis, structure, and stability of nanocrystalline materials have also been topics of many previous studies. Nanocrystalline materials are generally expected to be unstable thermodynamically, owing to the energy cost of their numerous internal interfaces. This thermodynamic instability can be mitigated by various kinetic or thermodynamic phenomena.¹⁻⁹ One suggestion was that a high entropy of the nanocrystalline microstructure could help stabilize it at finite temperatures.^{1,3,4} A large vibrational entropy of nanocrystalline microstructure was suggested by measurements of heat capacity,¹ although contamination by interstitial He atoms may have impaired these measurements.¹⁰ Measurements of Debye-Waller factors and Lamb-Mössbauer factors showed large mean-squared atomic displacements in nanocrystalline materials, suggesting that these materials may have large vibrational entropies.¹¹⁻¹⁵

More recently, inelastic scattering measurements with neutrons and γ rays have shown some differences in the phonon density of states (DOS) of nanocrystalline and bulk materials.¹⁶⁻²¹ One such effect was an enhancement of the phonon DOS at low energies.¹⁷⁻²¹ A second effect was a broadening of the phonon DOS.¹⁹⁻²¹ These effects are not well understood, and motivated the present, more extensive, inelastic neutron-scattering study on nanocrystalline Ni₃Fe. The alloy Ni₃Fe was chosen because it is possible to prepare it in nanocrystalline form in sufficient quantity for inelastic neutron-scattering measurements. The thermal neutron-scattering cross sections of Ni and Fe are large, and the lat-

tice dynamics are known for single crystals of fcc Ni₃Fe. Furthermore, preliminary measurements on this material showed large differences in the phonon DOS of nanocrystalline Ni₃Fe and a control sample having larger crystals.²⁰ For the present work the materials were prepared as disordered fcc solid solutions by high-energy ball milling, which was performed under two conditions to synthesize nanocrystallites of different sizes. Some of the powders were annealed to relieve internal stresses, or to cause growth of their crystallites. Inelastic neutron-scattering measurements were performed at 10 and 300 K to test for anharmonic effects in the phonon DOS.

To a first approximation, we found that the distortions of the phonon DOS were larger for materials with smaller crystallites. In particular, the enhancement of phonon DOS at low energies increased with the inverse of the crystallite size. This corresponds to a distortion of the phonon DOS that increases in proportion to the density of grain boundaries in the material. However, the broadening in energy of features of the phonon DOS could be altered by thermal treatments that had little effect on the crystallite size. We suggest that the broadening of the phonon DOS is a phenomenon with a different physical origin than the enhancement of the phonon DOS at low energies.

II. MATERIALS

Nanocrystalline nickel-iron powders were synthesized by the mechanical attrition of powders of Ni and Fe of 99.9% purity in a Spex 8000 mixer/mill with hardened steel vials and balls. One set of materials was milled for 6 h with a ball-to-powder weight ratio of 5:1 and 5 ml of ethanol. Another set was milled for 18 h with a ball-to-powder weight ratio of 20:1 and 2 ml of ethanol. Annealings at 265, 425, and 600 °C were performed on the powders milled with the

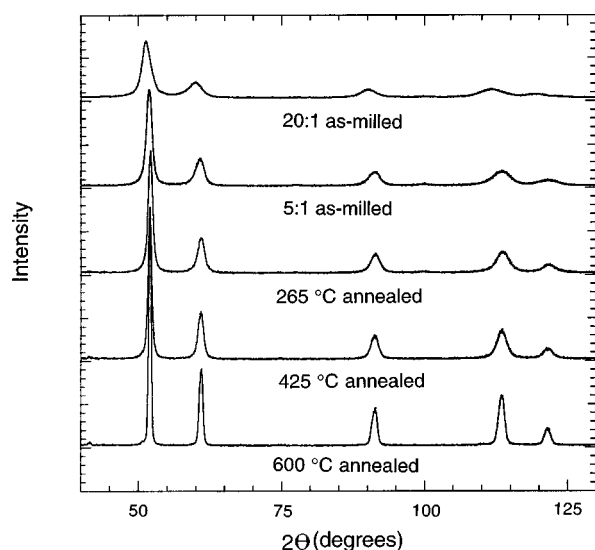


FIG. 1. X-ray-diffraction patterns of Ni₃Fe powders milled with ball-to-powder weight ratios of 20:1 and 5:1, and after annealing the 5:1 powder at the indicated temperatures.

5:1 ball-to-powder weight ratio. Owing to sluggish kinetics of ordering, it is unlikely that these annealings would produce any $L1_2$ order in the Ni₃Fe, and no superlattice diffractions were detected by x-ray diffractometry, nor by neutron diffractometry. Finally, although unexpected *a priori*, the material was also altered by cooling to 10 K in a displex refrigerator. A few grams of the powders were heated to 400 °C and analyzed for evolved hydrogen, oxygen, and nitrogen by a Hewlett-Packard 5890 gas chromatograph equipped with a thermal conductivity detector. No evolution of hydrogen was detected from heated samples of as-milled and annealed Ni₃Fe powder. Detection limits for hydrogen were better than 0.004 wt. %. We do not expect any significant quasielastic neutron scattering from hydrogen.

X-ray diffractometry was performed with an Inel CPS-120 diffractometer using Co $K\alpha$ radiation. Neutron diffractometry with neutrons of 1.50 Å wavelength was performed with the HB4 high-resolution powder diffractometer at the Oak Ridge National Laboratory. Figure 1 presents x-ray-diffraction patterns from the as-milled powders and from powders after annealing. Grain sizes and distributions of internal strains were obtained by the method of Williamson and Hall²² after correcting the x-ray peak shapes for the characteristic broadening of the x-ray diffractometer. Mean crystallite sizes were 6 nm for the material milled with a ball-to-powder weight ratio of 20:1, and 10 nm for material milled with a 5:1 ratio. After annealing the materials milled with a 5:1 ball-to-powder weight ratio, their mean grain (crystallite) sizes were 12 nm after 265 °C for 1.5 h, 15 nm after 425 °C for 1.5 h, and at least 25 nm after 600 °C for 1.5 h. From the slopes of the Williamson-Hall plots, the mean-squared strains were 0.4% in the material as-milled with a 5:1 ratio, and 0.1% in the annealed powders. The material as-milled with a 20:1 ratio had a mean-squared strain of less than 0.1%.

Both as-milled and annealed materials were studied by transmission electron microscopy (TEM) with a Philips EM 420 microscope operated at 120 keV. Samples were prepared by sprinkling some of the powders on holey carbon grids.

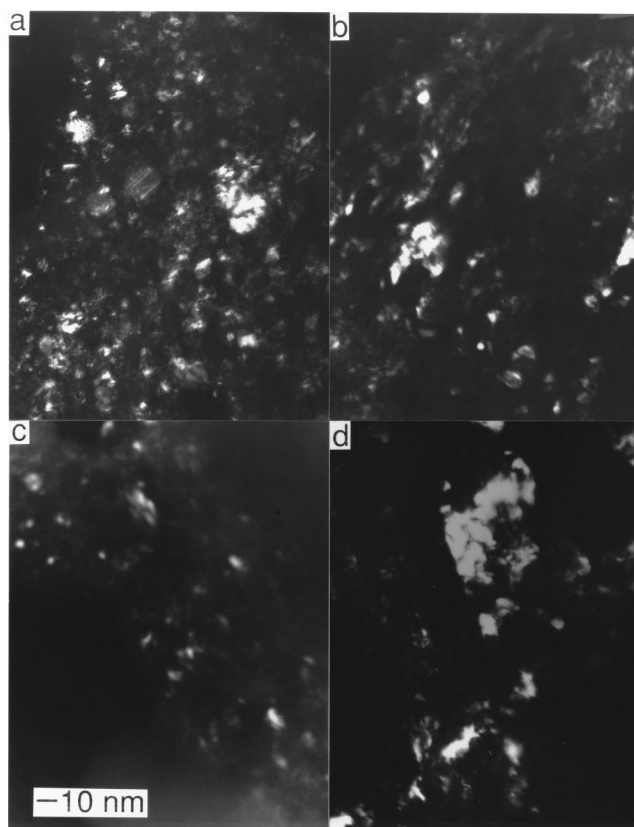


FIG. 2. Dark field transmission electron microscopy images of Ni₃Fe powders obtained with the (111) fcc diffraction. (a) as-milled with ball-to-powder weight ratio of 20:1, (b) as-milled with ratio of 5:1, (c) 5:1 powder annealed at 265 °C (d) 5:1 powder annealed at 600 °C.

Samples from earlier work²⁰ were prepared by embedding some of the powder in epoxy, and microtoming thin sections from the epoxy block. Sizes of the nanocrystals were determined by dark field imaging, which reveals a two-dimensional projection of the outer boundaries of the crystallites. Chemical analysis with an x-ray fluorescence spectrometer attached to the microscope showed little variation in the chemical composition within the powder particles. There was good agreement between the spectral intensities from these samples and the intensities from samples of Ni—25 at.% Fe prepared as an ingot by arc melting.

Bright field TEM images showed that the micron and sub-micron powder particles were dense and without internal porosity. The nanocrystals can be described as forming a three-dimensional mosaic tiling of the larger powder particles. Some dark field TEM images are presented in Fig. 2. These dark field images show a distribution in the crystallite (grain) sizes in the as-milled and annealed samples. Some extremely small crystallites are evident in the material as-milled with a ball-to-powder weight ratio of 20:1. Typical grain sizes of the powders milled with the 5:1 ratio were 6–10 nm, whereas the sample annealed at 600 °C had grain sizes of 50 nm and larger. This estimate of a 50 nm grain size from TEM should be more accurate than for x-ray diffraction since the x-ray linewidths from the sample annealed at 600 °C were comparable to the instrumental broadening. It is also important to note that the TEM dark field images show

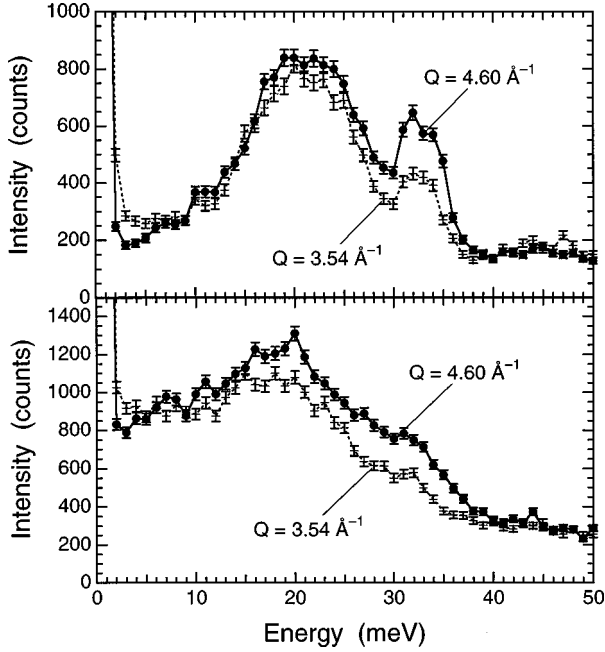


FIG. 3. Neutron energy loss spectra obtained with $Q = 3.54$ and 4.60 \AA^{-1} . Top: powder annealed at $600 \text{ }^\circ\text{C}$ (average crystallite size of 50 nm). Bottom: powder as-milled with ball-to-powder weight ratio of $20:1$ (average crystallite size of 6 nm).

the two-dimensional projections of diffracting crystallites, whereas line shapes in x-ray diffractometry are a volume average over all diffracting columns of crystallites.

Samples of the powders, each about 25 g , were placed in thin-walled vanadium cans and mounted in a dispex refrigerator on the goniometer of the HB3 triple axis spectrometer at the High Flux Isotope Reactor at the Oak Ridge National Laboratory. The spectrometer was operated in constant Q mode and a fixed final energy ε_f , of 14.8 meV . The energy-loss spectra were made by scanning the incident energy from 14.8 to 64.8 meV . The neutron flux from the monochromator was monitored with a fission detector, which was used to control the counting time for each data point. The incident beam on the pyrolytic graphite monochromator crystal had a collimation of $120'$, and $40'$ Soller slits were used between the monochromator and the sample. Pyrolytic graphite filters placed after the sample were used to attenuate the $\lambda/2$ and $\lambda/3$ contamination. The filtered beam passed through $40'$ slits before the pyrolytic graphite analyzer crystal. Following the analyzer, $80'$ Soller slits were used before the ^3He detector. With this arrangement, the energy resolution varied between 0.9 and 2 meV , depending on the energy transfer and the slope of the phonon dispersion surface. The elastic peak was found to have a full width at half maximum of 1.2 meV . Spectra from each specimen were obtained at two values of Q , 3.54 , and 4.60 \AA^{-1} . The choice of these two values of Q is discussed in the next section.

III. INELASTIC NEUTRON SCATTERING

Typical inelastic neutron scattering data are presented in Fig. 3. The analysis of the inelastic neutron-scattering data was helped considerably by results from previous coherent inelastic neutron-scattering studies on single crystals of

Ni_3Fe by Hallman and Brockhouse.²³ The lattice dynamics of fcc Ni_3Fe is similar to that of fcc Ni, even when the Ni_3Fe has $L1_2$ chemical order. Using the published force constants,²³ the dynamical matrix $\mathbf{D}(\mathbf{k})$ (Ref. 24) was diagonalized for approximately 10^6 values of \mathbf{k} distributed uniformly over the first fcc Brillouin zone. Histogram binning of the resulting eigenfrequencies provided the phonon DOS, presented in Fig. 4.

The dynamical structure factor intensity for incoherent scattering by phonons of energy ε , $|G_{\text{inc}}(\varepsilon, \mathbf{Q})|^2$, was obtained from the Born-von Kármán model as the following sum:²⁵

$$|G_{\text{inc}}(\varepsilon, \mathbf{Q})|^2 = \sum_{\mathbf{r}_k} \frac{\sigma_{\text{inc}, \mathbf{r}_k}}{M_{\mathbf{r}_k}} \sum_{\gamma} \sum_{\mathbf{q}} |\mathbf{Q} \cdot \mathbf{u}_{\mathbf{r}_k}^{\gamma}(\mathbf{q})|^2 \delta[\varepsilon - \varepsilon_{\gamma}(\mathbf{q})]. \quad (1)$$

The dynamical structure factor intensity for incoherent scattering, $|G_{\text{inc}}(\varepsilon, \mathbf{Q})|^2$, involves the projection of the momentum transfer \mathbf{Q} on the polarization vector $\mathbf{u}_{\mathbf{r}_k}^{\gamma}(\mathbf{q})$ for the atom of mass $M_{\mathbf{r}_k}$ at the position \mathbf{r}_k in the unit cell of the phonon with wave vector \mathbf{q} in the branch γ . Hallman and Brockhouse interpreted their data by assuming the lattice dynamics of an fcc alloy, so the atomic mass for all atoms was the average of that for $75\% \text{ Ni}$ and $25\% \text{ Fe}$, i.e., 58.0 g/mol . For each atom, branch, and \mathbf{q} , the crystallographic average of Eq. (1) over the various directions of \mathbf{Q} is $\sigma_{\text{inc}, \mathbf{r}_k} Q^2 |\mathbf{u}_{\mathbf{r}_k}^{\gamma}(\mathbf{q})|^2 / 3M_{\mathbf{r}_k}$. This contribution to $|G_{\text{inc}}(\varepsilon, \mathbf{Q})|^2$ was binned during the phonon DOS calculation.

The dynamical structure factor intensity for coherent scattering, $|G_{\text{coh}}(\varepsilon, \mathbf{Q})|^2$, was calculated as:²⁵

$$|G_{\text{coh}}(\varepsilon, \mathbf{Q})|^2 = \sum_{\mathbf{r}_k} \frac{1}{M_{\mathbf{r}_k}} \sum_{\gamma} \sum_{\tau} \sum_{\mathbf{q}} |b_{\mathbf{r}_k} \mathbf{Q} \cdot \mathbf{u}_{\mathbf{r}_k}^{\gamma}(\mathbf{q}) e^{i\mathbf{Q} \cdot \mathbf{r}_k}|^2 \times \delta[\varepsilon - \varepsilon_{\gamma}(\mathbf{q})] \delta(\mathbf{Q} - \mathbf{q} - \boldsymbol{\tau}), \quad (2)$$

where $\boldsymbol{\tau}$ is a reciprocal lattice vector and $b_{\mathbf{r}_k}$ is the coherent scattering length. The crystallographic average of the coherent inelastic scattering required an evaluation of the dynamical structure factor intensity at explicit values of \mathbf{Q} with respect to the crystallographic axes. For a given value of Q , the directions of \mathbf{Q} were chosen with an isotropic probability distribution using a Monte Carlo sampling procedure.¹⁷

Results for the total intensity of inelastic scattering, coherent plus incoherent, were summed by weighting the coherent contribution by 0.772 and the incoherent contribution by 0.228 to account for the average coherent and incoherent scattering of Ni_3Fe . Finally, the calculated inelastic scattering intensities for the two values of Q were added together and convoluted with a Gaussian function of full width at half maximum (FWHM) of 2.5 meV to account approximately for the experimental energy resolution. The result is shown as the dashed curve in Fig. 4. The solid curve is the actual phonon DOS of fcc Ni_3Fe , calculated with the Born-von Kármán model using the force constants of Hallman and Brockhouse, again convoluted with a Gaussian function of FWHM of 2.5 meV .

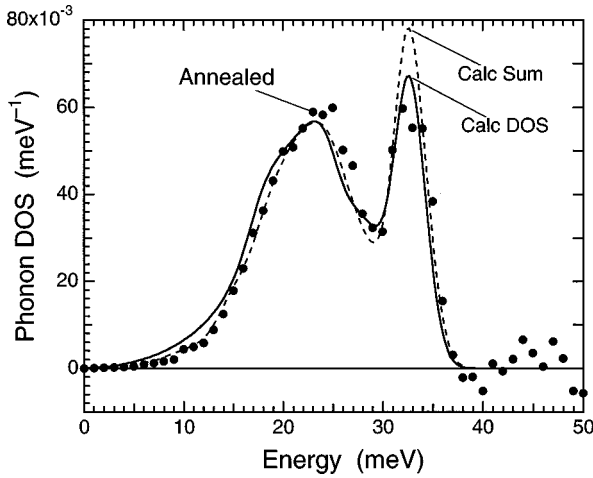


FIG. 4. Points: Experimental phonon DOS obtained for powder annealed at 600 °C. Solid curve: Calculated phonon DOS using the Born-von Kármán model with force constants of Ref. 23. Dashed curve: Calculated sum of dynamical structure factor intensities for $Q=3.54$ and 4.60 \AA^{-1} . Calculated curves were convoluted with a Gaussian resolution function of 2.5 meV full width at half maximum.

To obtain the approximate phonon DOS from the experimental spectra, the spectra measured with both values of $Q = 3.54$ and 4.60 \AA^{-1} were summed, and a constant background was then subtracted. The conventional multiphonon expansion^{26–28} was used to calculate the contributions to the inelastic scattering at 300 K. The results showed that the inelastic scattering is strongly dominated by one-phonon processes. Assuming the inelastic scattering $I(\varepsilon)$, is all one-phonon scattering, the phonon DOS, $g(\varepsilon)$, can be obtained from the inelastic spectrum as

$$g(\varepsilon) = \varepsilon [1 - \exp(-\varepsilon/kT)] I(\varepsilon). \quad (3)$$

The experimental phonon DOS curve obtained for the large-grained annealed sample is presented in Fig. 4 for comparison with the calculated DOS and the calculated sum of the dynamical structure factor intensities (which should provide a more accurate estimate of the experimentally derived spectrum).

IV. RESULTS AND DISCUSSION

A. General features of the phonon DOS

The experimental phonon DOS curves for most of the samples are presented in Fig. 5. We anticipated that the nanocrystalline materials would show an anharmonic softening of their phonon DOS curves, but we found no significant differences between the phonon DOS curves measured at 10 and at 300 K. (An irreversible change in the broadening of the phonon DOS curves of as-milled alloys after cryogenic exposure is described in Sec. IV C, however.) In comparison to the materials annealed at 600 °C, which has large crystals, the phonon DOS curves from the nanocrystalline material show two distinct differences. There is an increased intensity of the phonon DOS at energies below 15 meV. This excess intensity diminishes after the nanocrystalline materials are annealed at higher temperatures. The second difference is that the features of the phonon DOS are broadened in the

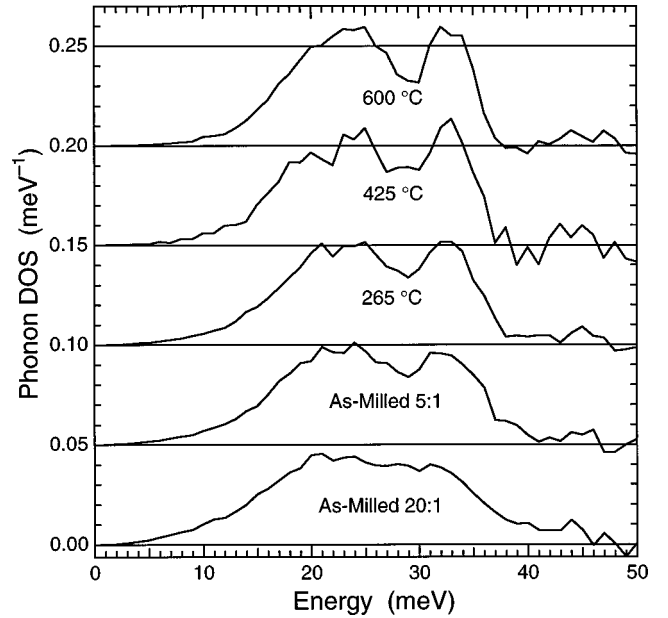


FIG. 5. Phonon DOS curves extracted from experimental data from Ni₃Fe powders milled with ball-to-powder weight ratios of 20:1 and 5:1, and after annealing the 5:1 powder at the indicated temperatures. Crystallite sizes were (top to bottom) 50, 15, 12, 10, and 6 nm.

nanocrystalline materials. Both these effects are also evident in raw data such as shown in Fig. 3. Although these two effects had been reported previously,^{17–21} the more systematic results of the present study allow for more detailed interpretations.

B. Features at low energies

Figure 6 shows the low-energy part of the phonon DOS curves $g(\varepsilon)$, presented in Fig. 5, with the data plotted against the square of the phonon energy. A quadratic dependence of the form

$$g(\varepsilon) = \alpha \varepsilon^2 \quad (4)$$

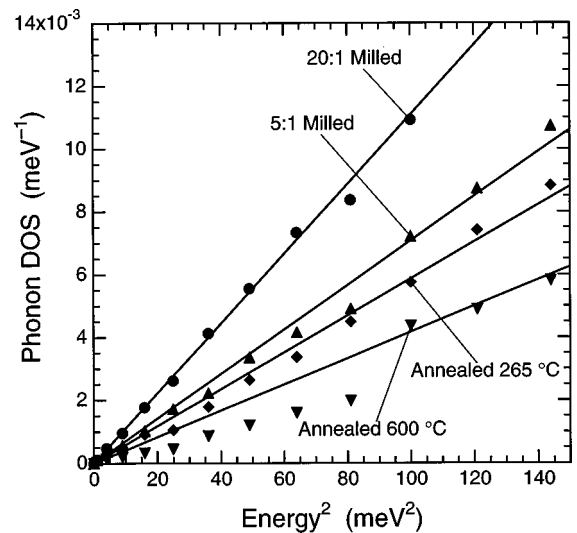


FIG. 6. Low-energy part of the phonon DOS curves of Fig. 5, graphed vs the square of energy.

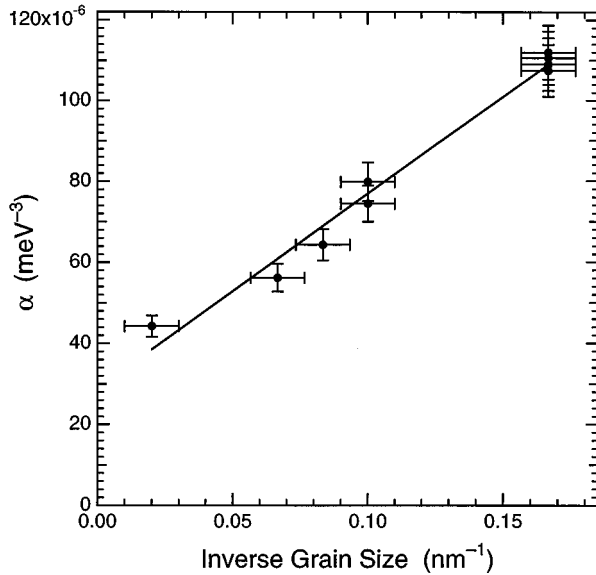


FIG. 7. Slopes of the lines shown in Fig. 6 [α of Eq. (4)] vs the inverse of the crystallite size.

is expected when the vibrational excitations in 3 dimensions have a constant group velocity, $h^{-1} \partial \epsilon / \partial q$. The function of Eq. (4) was fit to the data of Fig. 6 for the energy ranges 0–12, 0–13, and 0–14 meV, and the results averaged to obtain a value for α . This average α was plotted against the root-mean-squared (RMS) strains in the crystallites and against the grain size of the crystallites. The correlation with the RMS strain was poor, but the correlation against grain size was more monotonic. Provided the grain size distribution has the same functional form, but merely changes spatial scale with grain growth, the surface area of grain boundaries will depend on grain size d , as d^{-1} . In other words, the density of grain boundaries per unit volume may be expected to be proportional to the inverse of the grain size. This motivated us to plot in Fig. 7 the coefficient α of Eq. (4) against the inverse of the grain size. The linearity of this plot suggests that the enhancement of the phonon DOS at low energies is a phenomena related to the surfaces of the crystallites, such as surface modes. Tamura and co-workers²⁹ calculated the torsional and spheroidal vibrational modes of small spherical particles with relaxed surface zones. Model molecular dynamics calculations by this group³⁰ showed an enhanced phonon density of states at low energies, with general appearance similar to the DOS for the nanocrystalline material shown in Fig. 5. These surface modes will be altered when the particle is embedded in a matrix, but with an elastic discontinuity at the particle interfaces the concept of surface modes remains viable. The plot of Fig. 7 includes results from all measurements on as-milled and annealed materials. While the linearity is suggestive of a quantitative relationship, our measurements may not justify such a relationship in detail. In particular, the frequency spectrum of surface modes should depend on the nature of the contacts between crystallites, and these contacts probably change during annealing. It is also likely that the effective elastic constants of grain boundaries are different in the annealed materials. Such effects are not possible to estimate reliably.

The surface modes of adjacent crystallites will inevitably

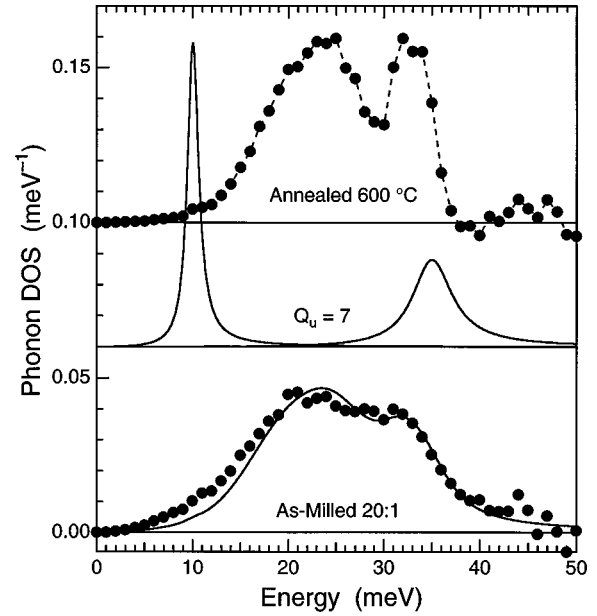


FIG. 8. The characteristic shape of the damped harmonic oscillator function is shown in the center of the figure for resonances at 10 and 35 meV having the quality factor $Q_u = 7$. Solid curve at bottom is the convolution of the damped harmonic oscillator function for $Q_u = 7$ with the experimental DOS from the sample annealed at 600 °C (points at top). Points at bottom are experimental DOS curve from 6 nm powder milled with a ball-to-powder weight ratio of 20:1.

interact with each other because propagation of vibrational energy between the crystallites is expected to occur through grain boundaries and interiors. The simplest picture would be for an intercrystalline transmission of rigid unit displacements and rotations of the crystallites. There are, however, relatively few such rigid unit modes when the crystallites contain 10^4 atoms. We do expect, however, that the grain boundaries will serve to propagate surface mode vibrations between the crystallites. If the grain boundaries served as springs with weak spring constants, the intracrystalline vibrations would differ in phase between neighboring crystallites.

A different viewpoint has been provided for understanding the vibrational spectrum of amorphous materials.^{31–34} Local regions having low-frequency vibrations may interact by absorbing and rescattering vibrational waves from the surrounding matrix.³⁴ Perhaps some of the heterogeneities in our nanocrystalline materials could act as low-frequency resonators. A model of scattering of matrix phonons by local regions with low resonant frequencies seems unlikely to provide the linear slopes of Fig. 6, since this model tends to show a “Boson peak” when $g(\epsilon)\epsilon^{-2}$ is plotted against ϵ .

C. Features at higher energies

Figure 8 compares the experimental phonon DOS for our nanocrystalline material with the smallest crystallite size to the DOS for the annealed material with the largest crystallite size. In addition to the enhanced intensity at low energies, discussed in the previous section, there is a broadening in energy of the nanocrystalline phonon DOS. In particular, a tail extends to high energies. As a possible interpretation of

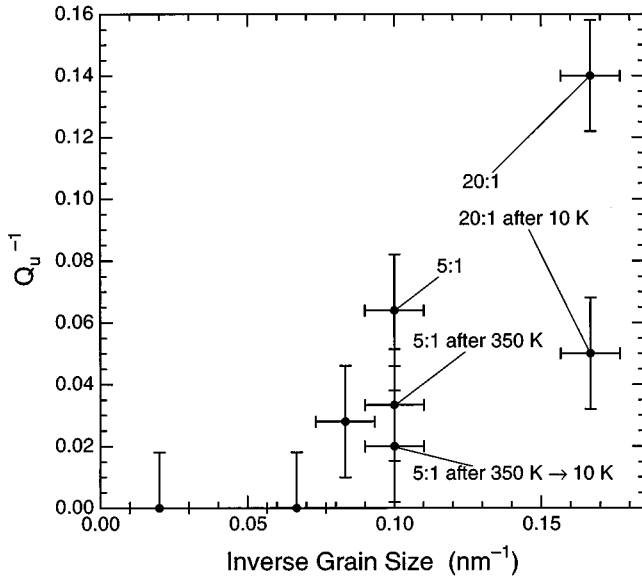


FIG. 9. Inverse of the quality factor Q_u , vs the inverse of crystallite size. Labels indicate additional treatments given to the samples.

this broadening, we calculated the phonon DOS for the nanocrystalline material with the assumption that each phonon was broadened in energy as a damped harmonic oscillator. Damped harmonic oscillator functions for phonons at 10 and 35 meV with oscillator quality factors³⁵ $Q_u=7$ are shown in the middle of Fig. 8. To obtain the solid curve at the bottom of Fig. 8, each intensity at the energy ε' of the experimental DOS curve of the annealed material was convoluted with the characteristic spectrum of a damped harmonic oscillator

$$D_{\varepsilon'}(\varepsilon) = \frac{1}{\pi Q_u \varepsilon'} \frac{1}{\left(\frac{\varepsilon' - \varepsilon}{\varepsilon - \varepsilon'}\right)^2 + \frac{1}{Q_u^2}}. \quad (5)$$

The only free parameter in fitting the phonon DOS from the nanocrystalline material was Q_u , which was assumed to be the same for all phonons. The solid curve at the bottom of Fig. 8 was obtained with a value of $Q_u=7$. Many features of the phonon DOS of the nanocrystalline material are represented well by this assumption of a damped harmonic oscillator. The shape of the high-energy tail above the longitudinal peak is modeled particularly well, as is the suppressed dip between the transverse and longitudinal bands of states. The enhanced low-energy part of the phonon DOS of the nanocrystalline material, discussed in the previous section, evidently does not originate from phonon damping of this type.

The amount of damping, parametrized as Q_u^{-1} , is presented in Fig. 9 vs the inverse crystallite size. The systematics are not so consistent as for the enhanced phonon DOS at low energies (Fig. 7). This difference indicates that the damping has a different origin. In particular, the damping can be changed significantly by thermal treatments of the sample which have no effect on the grain size, such as low-temperature annealings and exposure to cryogenic temperatures. An unexpected effect of cryogenic exposure is shown

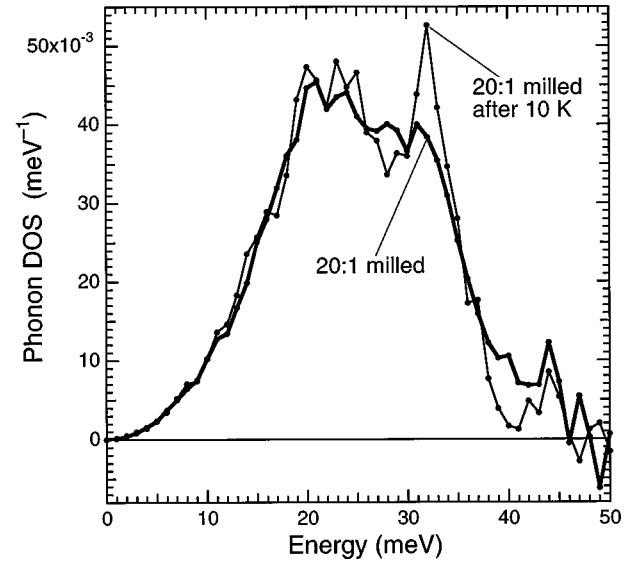


FIG. 10. Effect of cryogenic exposure on the experimental phonon DOS curve at 300 K of the 6 nm material milled with a ball-to-powder weight ratio of 20:1.

in Fig. 10 with experimental DOS curves of the material milled with the ball-to-powder weight ratio of 20:1 (6 nm crystallites). Notice that the longitudinal peak in the phonon DOS of the as-milled nanocrystalline material is sharpened significantly after the sample was exposed to cryogenic temperature. Some sharpening of the transverse band of states may also occur. On the other hand, the enhanced phonon DOS at low energies is little changed. This sharpening of the phonon DOS was irreversible. It was observed when the material was first cooled to 10 K, and remained after warming to 300 K. The phonon DOS curves obtained from the spectra measured at 10 K and after warming to 300 K were the same within experimental error. A similar sharpening of the longitudinal peak of the phonon DOS was observed after the material milled with the 5:1 ball-to-powder weight ratio was annealed at 350 K for 8 h, and this sharpening became more pronounced after this 5:1 material was exposed to a temperature of 10 K.

To study further this effect of cryogenic exposure on the phonon damping, we compared x-ray-diffraction patterns of as-milled powders before and after immersion in liquid nitrogen at 77 K and liquid helium at 4 K for 45 min. The diffraction patterns were identical within experimental error, indicating that changes in crystallite size or residual stress in the material are probably not responsible for the change in the phonon DOS after cryogenic exposure. On the other hand, low-temperature annealings or cryogenic exposures could cause changes in local atomic structures of grain boundaries by causing the reconfiguration of those atoms in energetically unfavorable local environments. Such changes would not be evident in our x-ray-diffraction patterns, but these changes would be expected to affect the anharmonic character of the vibrations of grain-boundary atoms. A large anharmonicity in as-milled materials would intermix phonons of different energies, and this would be evident as damping. If cryogenic exposure or low-temperature annealing were to reduce the local atomic distortions in grain boundaries and thereby reduce the anharmonic nature of the

interatomic potential, the phonon damping would be diminished. We note that a recent study on vibrations in nanocrystalline ^{57}Fe that had a large amount of free surface also showed evidence for large phonon damping.²¹

An alternative explanation for vibrational modes at high energies was suggested by D. Wolf *et al.*³⁶ Their molecular dynamics simulations showed that nanocrystalline materials had low-energy modes associated with grain boundaries, approximately consistent with our results of Fig. 5. The molecular dynamics simulations also showed modes at energies above those of the crystallites. These high-energy modes were attributed to local atomic environments in grain boundaries with reduced interatomic separations. This explanation seems consistent with our observations, assuming again that cryogenic exposure or low-temperature annealing were to reduce the local atomic distortions within grain boundaries.

D. Vibrational entropy

Vibrational entropy has been proposed as a reason for the thermal stability of nanocrystalline materials at moderate temperatures.^{1,3,4} We define $\Delta S_{\text{vib}} \equiv S_{\text{vib}}^{\text{nan}} - S_{\text{vib}}^{\text{blk}}$ as the difference in vibrational entropy of nanocrystalline and annealed Ni_3Fe . At high temperatures this difference in vibrational entropy depends in a straightforward way on the difference in the vibrational DOS of the two phases, $g^{\text{nan}}(\varepsilon) - g^{\text{blk}}(\varepsilon)$.^{17,19}

$$\Delta S_{\text{vib}} = -3k_B \int_0^\infty [g^{\text{nan}}(\varepsilon) - g^{\text{blk}}(\varepsilon)] \ln(\varepsilon) d\varepsilon, \quad (6)$$

where the difference avoids problems with the dimensions of the argument of the logarithm. Using the DOS curves of Fig. 5, for high temperature we find that the vibrational entropy of the 20:1 as-milled alloys is larger by about $0.10 k_B/\text{atom}$ than for the sample annealed at 600°C . On the other hand, the vibrational entropy of the 5:1 material is essentially the same as that of the 600°C annealed sample. Subsequent annealings at 265 and 425°C caused little change in the vibrational entropy of the 5:1 powder. Studies on other nanocrystalline materials reported vibrational entropies up to $0.2 k_B/\text{atom}$ larger than their bulk counterparts.^{17,19,20} These other nanocrystalline materials also had significant enhancements of their phonon DOS at low energies. In the present nanocrystalline alloys, surprisingly, the large lifetime broadening of the DOS to high energies largely cancels the effects from the enhancement of the phonon DOS at low energies. On the other hand, by annealing at low temperature or by cryogenic exposure it was possible to soften the high-energy part of the phonon DOS in the as-milled materials without affecting the phonon DOS at low energy. The sharpening of

the high-energy part of the DOS after the 10 K quench or after annealing at 350 K caused the vibrational entropy of the 5:1 alloy to increase by about $0.11 k_B/\text{atom}$. The 10 K quench caused the vibrational entropy of the 20:1 to increase by about $0.05 k_B/\text{atom}$. Vibrational entropy should have only a modest effect on the thermodynamic stability of our nanocrystalline Ni_3Fe . For comparison, at 400 K a difference in vibrational entropy of $0.1 k_B/\text{atom}$ contributes approximately 300 J/mol to the free-energy difference, which is several times smaller than the grain-boundary enthalpy.

V. CONCLUSIONS

Inelastic neutron-scattering spectra were measured from nanocrystalline Ni_3Fe prepared by mechanical alloying, and from these materials after thermal treatments. The spectra measured at constant Q were converted into approximate phonon DOS curves. Compared to the same alloy having large crystallites, the nanocrystalline materials had (1) an enhancement of their phonon DOS at low energies, and (2) a broadening of their phonon DOS, most notably at high energies. Although these features were reported previously, the present study was performed on a variety of samples with different crystallite size. The enhancement of the phonon DOS at low energies was especially large in samples with the smallest average crystallite size, but this enhancement decreased with crystallite size d , as d^{-1} . There was no distinct structure in this low-energy part of the phonon DOS, and the intensity increased with phonon energy ε , approximately as ε^2 . The broadening of the phonon DOS did not show a simple dependence on crystallite size. This broadening could be modeled successfully as a damping of the vibrational modes. Large reductions in this broadening were obtained with mild thermal treatments of the sample—annealing at 350 K or exposure to 10 K . We suggest that the broadening of the phonon DOS originates with anharmonic interatomic potentials in unrelaxed grain boundaries. We did not observe other anharmonic effects, however, such as a softening of the phonon DOS between 10 and 300 K . Finally, we note that the effects on the vibrational entropy from these two features of the phonon DOS of the nanocrystalline material tend to cancel each other.

ACKNOWLEDGMENTS

The Oak Ridge National Laboratory is managed for the Department of Energy by Lockheed Martin Energy Research, Oak Ridge, TN under Contract No. DE-AC05-96OR22464. This work was supported by the U.S. Department of Energy under Contract No. DE-FG03-96ER45572.

¹See, for example, H. Gleiter, *Prog. Mater. Sci.* **33**, 223 (1989).

²See, for example, R. W. Siegel, *Phys. Today* **46**, 64 (1993).

³H. J. Fecht, *Phys. Rev. Lett.* **65**, 610 (1990).

⁴M. Wagner, *Acta Metall. Mater.* **40**, 957 (1992).

⁵Y. R. Abe, J. C. Holzer, and W. L. Johnson, in *Structure and*

Properties of Interfaces in Materials, edited by W. A. T. Clark, U. Dahmen, and C. L. Briant (Materials Research Society, Pittsburgh, 1992), p. 721.

⁶J. Weissmüller, *J. Mater. Res.* **9**, 4 (1994).

⁷Z. Q. Gao and B. Fultz, *Nanostruct. Mater.* **4**, 939 (1994); C.

- Bansal, Z. Q. Gao, and B. Fultz, *ibid.* **5**, 327 (1995).
- ⁸C. D. Terwilliger and Y.-M. Chiang, *Acta Metall. Mater.* **43**, 319 (1995).
- ⁹C. E. Krill, H. Ehrhardt, and R. Birringer, in *Chemistry and Physics of Nanostructures and Related Non-Equilibrium Materials*, edited by E. Ma, B. Fultz, T. Shull, J. Morral, and P. Nash (TMS, Warrendale, PA, 1997), p. 115.
- ¹⁰A. Tschöpe and R. Birringer, *Acta Metall. Mater.* **41**, 2791 (1993).
- ¹¹G. Von Eynatten, J. Horst, K. Dransfeld, and H. E. Bömmel, *Hyperfine Interact.* **29**, 1311 (1986).
- ¹²H. Kuwano, H. Ouyang, and B. Fultz, *Nanostruct. Mater.* **1**, 143 (1992).
- ¹³J. A. Eastman and M. R. Fitzsimmons, *J. Appl. Phys.* **77**, 522 (1995).
- ¹⁴M. Hayashi, E. Gerkema, E. M. van der Kraan, and I. Tamura, *Phys. Rev. B* **42**, 9771 (1990).
- ¹⁵L. B. Hong, C. C. Ahn, and B. Fultz, *J. Mater. Res.* **10**, 2408 (1995).
- ¹⁶K. Suzuki and K. Sumiyama, *Mater. Trans. JIM* **36**, 188 (1995).
- ¹⁷B. Fultz, L. Anthony, L. J. Nagel, R. M. Nicklow, and S. Spooner, *Phys. Rev. B* **52**, 3315 (1995).
- ¹⁸J. Trampenau, K. Bauszuz, W. Petry, and U. Herr, *Nanostruct. Mater.* **6**, 551 (1995).
- ¹⁹B. Fultz, J. L. Robertson, T. A. Stephens, L. J. Nagel, and S. Spooner, *J. Appl. Phys.* **79**, 8318 (1996).
- ²⁰H. N. Frase, L. J. Nagel, J. L. Robertson, and B. Fultz, *Philos. Mag. B* **75**, 335 (1997).
- ²¹B. Fultz, C. C. Ahn, E. E. Alp, W. Sturhahn, and T. S. Toellner, *Phys. Rev. Lett.* **79**, 937 (1997).
- ²²H. P. Klug and L. E. Alexander, *X-Ray Diffraction Procedures* (Wiley-Interscience, New York, 1974), pp. 656 and 664.
- ²³E. D. Hallman and B. Brockhouse, *Can. J. Phys.* **47**, 1117 (1969).
- ²⁴G. Venkataraman, L. A. Feldkamp, and V. C. Sahni, *Dynamics of Perfect Crystals* (MIT Press, Cambridge, 1975), Chap. 2.
- ²⁵G. Kostorz and S. W. Lovesey, in *Treatise on Materials Science and Technology Vol. 15 Neutron Scattering*, edited by G. Kostorz (Academic, New York, 1979), p. 1.
- ²⁶V. F. Sears, *Phys. Rev. A* **7**, 340 (1973).
- ²⁷G. L. Squires, *Introduction to the Theory of Thermal Neutron Scattering* (Cambridge University Press, Cambridge, 1979), pp. 54–58.
- ²⁸V. F. Sears, E. C. Svensson, and B. M. Powell, *Can. J. Phys.* **73**, 726 (1995).
- ²⁹A. Tamura, K. Higeta, and T. Ichinokawa, *J. Phys. C* **15**, 1585 (1983); **16**, 4975 (1983).
- ³⁰A. Tamura and T. Ichinokawa, *J. Phys. C* **16**, 4779 (1983).
- ³¹M. F. Thorpe, *J. Non-Cryst. Solids* **57**, 355 (1983).
- ³²T. Pang, *Phys. Rev. B* **45**, 2490 (1992).
- ³³M. I. Klinger, *Phys. Lett. A* **170**, 222 (1992).
- ³⁴D. Caprion, P. Jund, and R. Jullien, *Phys. Rev. Lett.* **77**, 675 (1996).
- ³⁵A. P. French, *Vibrations and Waves* (Norton, New York, 1971), p. 99.
- ³⁶D. Wolf, J. Wang, S. R. Phillpot, and H. Gleiter, *Phys. Rev. Lett.* **74**, 4686 (1995).